CHAPTER 3

Cell Life Cycle Effects of Bare and Coated Superparamagnetic Iron Oxide Nanoparticles

Morteza Mahmoudi[1,2*], Sophie Laurent[3] and W. Shane Journeay[4,5]

[1]National Cell Bank, Pasteur Institute of Iran, Tehran, Iran; [2]Institute for Nanoscience and Nanotechnology, Sharif University of Technology, Tehran, Iran; [3]Department of General, Organic, and Biomedical Chemistry, NMR and Molecular Imaging Laboratory, University of Mons, Belgium; [4]Nanotechnology Toxicology Consulting and Training, Inc, Nova Scotia, Canada and [5] Faculty of Medicine, Dalhousie Medical School, Dalhousie University, Halifax, Nova Scotia, Canada

Abstract: Due to the hopeful potential of nanoparticles in medicine, they have attracted much attention for various applications such as targeted drug/gene delivery, separation or imaging. Interaction of NPs with the biological environment can lead to a wide range of cellular responses. In order to have safe NPs for biomedical applications, the current biocompatibility researches are particularly focused on the severe toxic mechanisms which cause cells death. These mechanisms are apoptosis, autophagy and necrosis, which can also be intricately linked with the cell-life cycle, as there are various check-points and controls in a cell's life cycle to ensure appropriate division processes. Mechanisms by which toxicants induce cell death by necrosis and apoptosis have been the focus of many biomedical disciplines because it helps us understand toxicity but also provides opportunities for drugs to impact on dysregulation of the cell cycle in diseases such as cancer. Among various types of NPs, the superparamagnetic iron oxide nanoparticles (SPION) are recognized as powerful biocompatible materials for multi-task nanomedicine applications such as drug delivery, magnetic resonance imaging, cell/protein separation, hyperthermia and transfection. This chapter presents overview of the effect of SPION on the cell life cycle.

Keywords: Superparamagnetic iron oxide nanoparticles, Cell cycle, TUNEL assay, Protein absorption, Polyethylene glycol fumarate, Polyvinyl alcohol, Propidium iodide, Phosphate buffer saline, Fetal bovine serum, MTT assay, Derivative study.

CELL LIFE CYCLE

The cell life cycle corresponds to a series of events which lead the cell to its division, duplication, and death [1-5]. Cell-life phases are divided into three main parts including G_1, S, and G_2. In the first gap phase (G_1), the cell grows and produces enzymes that are necessary for cell division. In the synthesis phase (S), the DNA is replicated. In the second gap phase (G_2), the cell continues to grow and the cell is carrying out processes necessary for mitosis (M). In both the G_1 and G_2 phases, there are checkpoints that ensure appropriate criteria are met for cycle progression. The effect of NPs on cells depends on their physiochemical properties such as size and distribution, shape, and charge [6]. One adverse effect of certain NPs is the induction of oxidative stress in treated-cells, causing the potential for DNA damage as an early effect evidenced in cell cycle progression. DNA damage is divided into reversible and irreversible types. Considering the cells with reversibly damaged DNA, the cells will accumulate in the G_1, or S, and in the G_2/M phases [7]. Cells which carry irreversibly damaged DNA will proceed to apoptosis, giving rise to the formation of fragmented DNA that can be identified in the subG_1 phase [8].

The cell cycle is a vital process for removal of the damaged cells (via apoptosis) and the disruption of this regulated process can induce the formation of tumors. More specifically, some genes like the cell cycle inhibitors (*e.g.*, RB, p53) when they mutate, can cause the cell to multiply uncontrollably, forming a tumor. Although the duration of cell cycle in tumor cells is equal to or longer than that of normal cell cycle, the

Address correspondence to Morteza Mahmoudi: National Cell Bank, Pasteur Institute of Iran, 69 Pasteur Ave. Kargar Ave., Tehran, Iran; Tel: +989125791557; E-mail: mahmoudi@biospion.com

Haseeb Ahmad Khan and Ibrahim Abdulwahid Arif (Eds)

proportion of cells that are in active cell division (versus quiescent cells in G_0 phase) in tumors is much higher than that in healthy tissue. Thus there is a net increase in cell number as the number of cells that die by apoptosis or senescence remains the same. The cells which are actively undergoing cell cycle transition are targeted in cancer therapy as the DNA is relatively exposed during cell division and hence susceptible to damage by drugs or radiation. This physiology is exploited in cancer treatment by a process known as debulking, whereby a significant mass of the tumor is removed which pushes a number of the remaining tumor cells from G_0 to G_1 phase.

SPION

SPION are classified as inorganic-based NPs having an iron oxide core coated by both inorganic and organic materials. There are two types of iron oxides including magnetite (Fe_3O_4) and maghemite (γ-Fe_2O_3), however the magnetite has attracted scientists due to its greater biocompatibility in comparison to maghemite [9, 10]. The favorable inorganic coatings are limited to silica and gold, however there are wide range of organic coatings such as polymers (*e.g.*, polyethylene glycol, polyethylene glycol fumarate (PEGF), and polyvinyl alcohol), acrylates, phospholipids, fatty acids, polysaccharides, and peptides [11]. In comparison with other NPs, SPION have the capability to target a desired site or to heat in the presence of an externally applied AC magnetic field, due to their inducible magnetization. More specifically, SPION have been recognized as a very promising kind of NPs not only due to their very good biocompatibility [11-17], but also due to their diversity of potential applications which can significantly increase patient compliance [18-20].

The SPION have been extensively employed for both *in vitro* and *in vivo* biomedical applications such as magnetic resonance imaging (MRI) contrast enhancement [21, 22], tissue specific release of therapeutic agents [23], hyperthermia, transfection, cell/biomolecules separation, and targeted drug delivery [24]. Many SPION such as Feridex, Endorem or Combidex are commercial and have the FDA approval for MR imaging [25, 26]. The current approaches in SPION are focused on their usage in *'theragnositc'* (*i.e.*, therapeutic and diagnostic) applications.

EFFECT OF SPION ON CELL LIFE CYCLE

The effects of different SPION on the cell-life cycle of various cells are summarized in Table **1**. Preliminary SPION formulations have shown to induce both reversible and irreversible DNA damage. For example, the toxic effects of bare SPION, with both magnetite and maghemite structures, on the A549

Table 1: Effect of SPION on the cell-life assay.

Coating	Size (nm)	Cell Type	Exposure		Phase Arrest	Phase Enhanced	Remark	Refs.
			Conc.	Time (h)				
Polyvinyl alcohol	48	Mouse tissue connective	80 mM	72	None	G_2/M	Surface passivated nanoparticles were used.	[7]
None	4.5	Mouse tissue connective	80 mM	72	None	Sub G_0G_1 and G_2/M	Surface passivated nanoparticles were used.	[7]
Polyvinyl alcohol	12	Mouse tissue connective	200-400 mM	72	None	None	Surface Active nanoparticles were used.	[13]
None	4	Mouse tissue connective	200-400 mM	72	G_0G_1	Sub G_0G_1	Surface Active nanoparticles were used.	[12, 13]
Carboxy-dextran	45-60	human mesenchy-mal stem cells	300 µg/ml	1	None	S and G_2/M	SPION-promoted cell growth is due to its ability to diminish intracellular H_2O_2 through intrinsic peroxidase-like activity.	[35]

human lung epithelial cell line were probed. The abilities of these magnetic nanoparticles to cause DNA damage and oxidative lesions have been evaluated using the comet assay [27]. The intracellular production of reactive oxygen species (ROS) was also measured by the oxidation sensitive fluoroprobe 2',7'-dichlorofluorescin diacetate and the observed toxicity ranged from none to low. Neither DNA damage nor intracellular ROS toxic effects in human lung cells were seen from interaction with magnetite nanoparticles at concentrations of 20-40 μg/mL. However, low quantities of oxidative DNA lesions were observed. There are several methods to track the effects of the DNA damage on the cell-life cycle phases such as the TUNEL (terminal deoxynucleotidyl transferase-mediated dUTP nick end-labeling) assays, which will be described later in this chapter.

APOPTOSIS MEASUREMENT

The apoptosis phenomenon occurs due to the irreversible DNA damages. A ubiquitous feature of the apoptosis phenomenon is the breakup of chromatin, which happens during the exposure of numerous 3′ OH DNA ends. By analyzing the DNA of cells which are undergoing apoptosis, using gel electrophoresis, a unique ladder-like appearance of DNA pieces with discrete molecular weights is observed. Hence, a reliable and rapid method for apoptosis evaluation is to compare the mobility of DNA extracted from control and apoptotic cells, for instance comparing DNA mobility of untreated Jurkat cells to the mobility of DNA of camptothecin-induced Jurkat cells [28, 29]. To determine apoptosis due to the exposure of cells to the SPION, there are several commercialized kits such as Apoptosis APO-BRDUTM kit (Sigma-Aldrich, Inc.) which needs dual color flow cytometry method for its evaluation.

Typically, BRDUTM kit provides a simple process of assessing apoptosis; however, the use of this kit requires that the cells are lysed. The appearance of the 3′ OH ends can also be quantified as a measurement of apoptosis in whole cells by an alternative method which does not require cell lysis. An alternative method in mixed cell populations is called the TUNEL assay, also known as the bromodeoxyuridine terminal deoxynucleotidyl transferase assay. For instance, the L929 mouse fibroblasts connective tissue cells were treated with both bare and polyvinyl alcohol (PVA)-coated SPION and their apoptotic effects were tracked with the TUNEL assay [12]. In order to prepare both control and treated-cells for flow cytometry evaluations, the predetermined cells were fixed with paraformaldehyde in PBS, followed by ethanol fixation. Consequently, the cells were washed and reacted with the TdT enzyme (terminal deoxynucleotidyl transferase) and Br-dUTP (bromodeoxyuridine triphosphate) in buffered solution at 37°C for 60 min. In this case, bromodeoxyuridine was covalently incorporated into the 3′ DNA ends during this incubation. Cells should be then thoroughly rinsed and incubated with a FITC (fluorescein isothiocyanate) labeled antibody directed to bromodeoxyuridine for about 30 min. After washing away unbound antibody, immunostaining with the FITC labeled anti-bromodeoxyuridine antibody allowed to determine the number of free 3′ ends. The RNA of the cells was then digested and the total DNA stained by incubation with a solution containing RNase A plus propidium iodide. Staining of cells with propidium iodide allows normalizing FITC staining to the total amount of DNA in the cells. Finally, the stained cells were analyzed by flow cytometry with an argon laser emitting at 488 nm. FITC fluorescence was observed at 520 nm and propidium iodide simultaneously at 623 nm. The results shown in Fig. **1** indicated that the SPION treated-cells did not show apoptosis at the examined SPION content up to concentrations of 200 mM.

CELL CYCLE ASSAY

Cell cycle assay could be evaluated by staining of the DNA with the suitable fluorescence dyes, such as propidium iodide (PI), followed by flow cytometric measurement of the fluorescence. Typically, the cells were cultured and then treated with the NPs for the desired time. Since the damaged cells may leave their attached places and be suspended in medium, the medium should be stored after removal.

Then, the remaining adhesive cells could be detached from the flask *via* trypsin treatment and harvested using the stored medium followed by centrifugation at about 280 G. The collected cells were washed thoroughly with phosphate buffer saline (PBS) followed by transferring of cells into the tubes containing 70% ethanol for fixation and stored at -20°C. Prior to the flow cytometric analysis, the ethanol-suspended cells were centrifuged

at 200g for about 5 min and the supernatants were decanted comprehensively. The collected cells were washed with PBS and then suspended in 1 ml PI/Triton X-100 staining solution with RNase A at 37°C for 15 min or at ambient temperature for 30 min. The stained cells are then ready for evaluations by flow cytometry at an excitation wavelength of 488 nm (for PI) and emission wavelength of 610 nm.

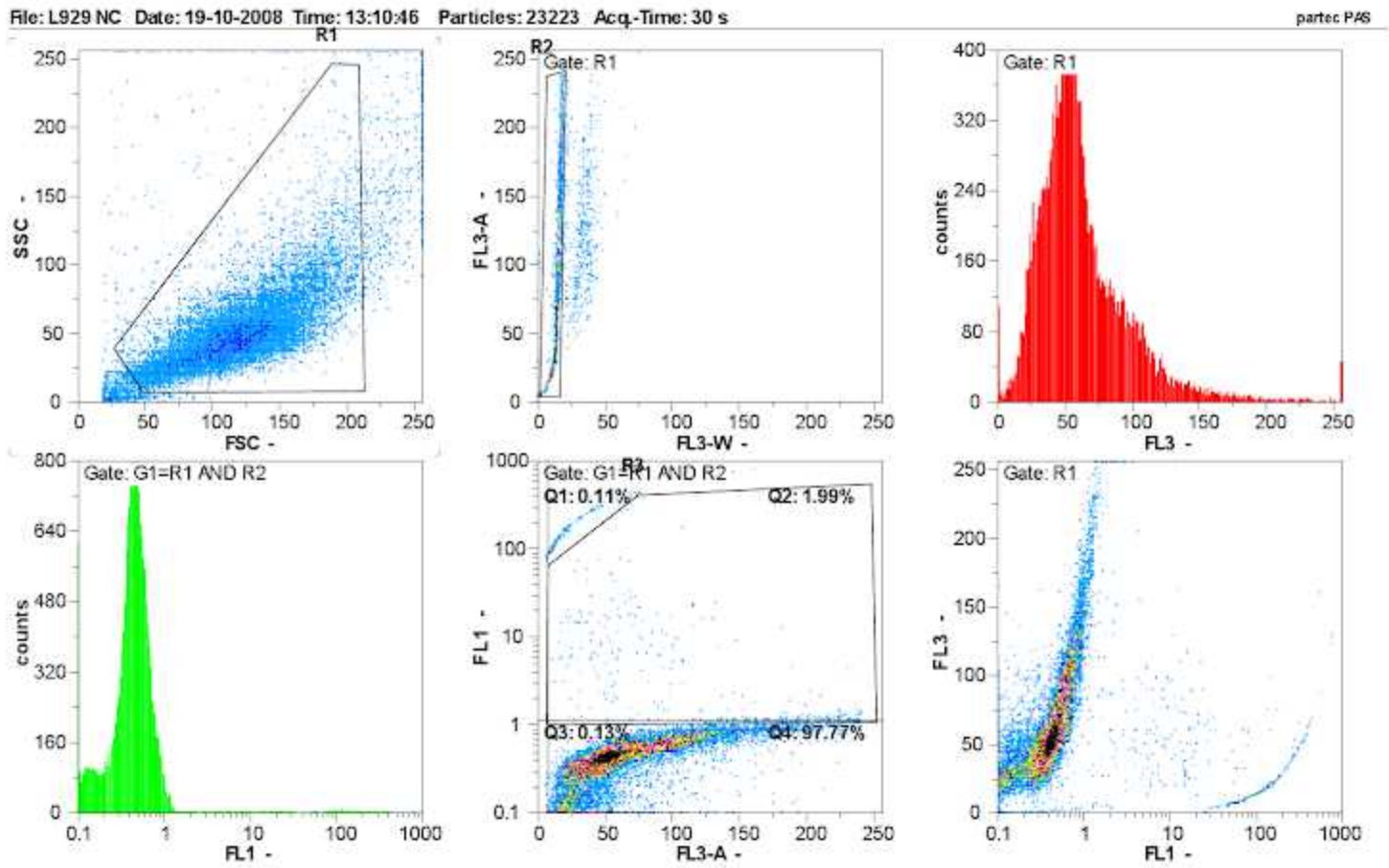

Region	Gate	Ungated	Count	Count/ml	%Gated	GMn-x	Mean-x	CV-x%	GMn-y	Mean-y	CV-y%
R1	<None>	21209	21209	-	91.33	112.77	118.46	29.83	45.94	50.74	47.09
R2	R1	20786	20276	-	95.60	13.83	14.00	13.92	54.82	63.78	57.46
Q1	G1	708	22	-	0.11	6.81	6.83	7.37	76.52	78.71	17.05
Q2	G1	1140	404	-	1.99	50.65	79.65	90.46	17.22	81.39	148.31
Q3	G1	656	26	-	0.13	6.94	6.97	9.46	0.12	0.13	41.77
Q4	G1	20719	19824	-	97.77	55.19	63.59	55.71	0.40	0.45	43.66
R3	G1	535	336	-	1.66	101.10	127.82	57.09	3.07	9.36	320.24

(a)

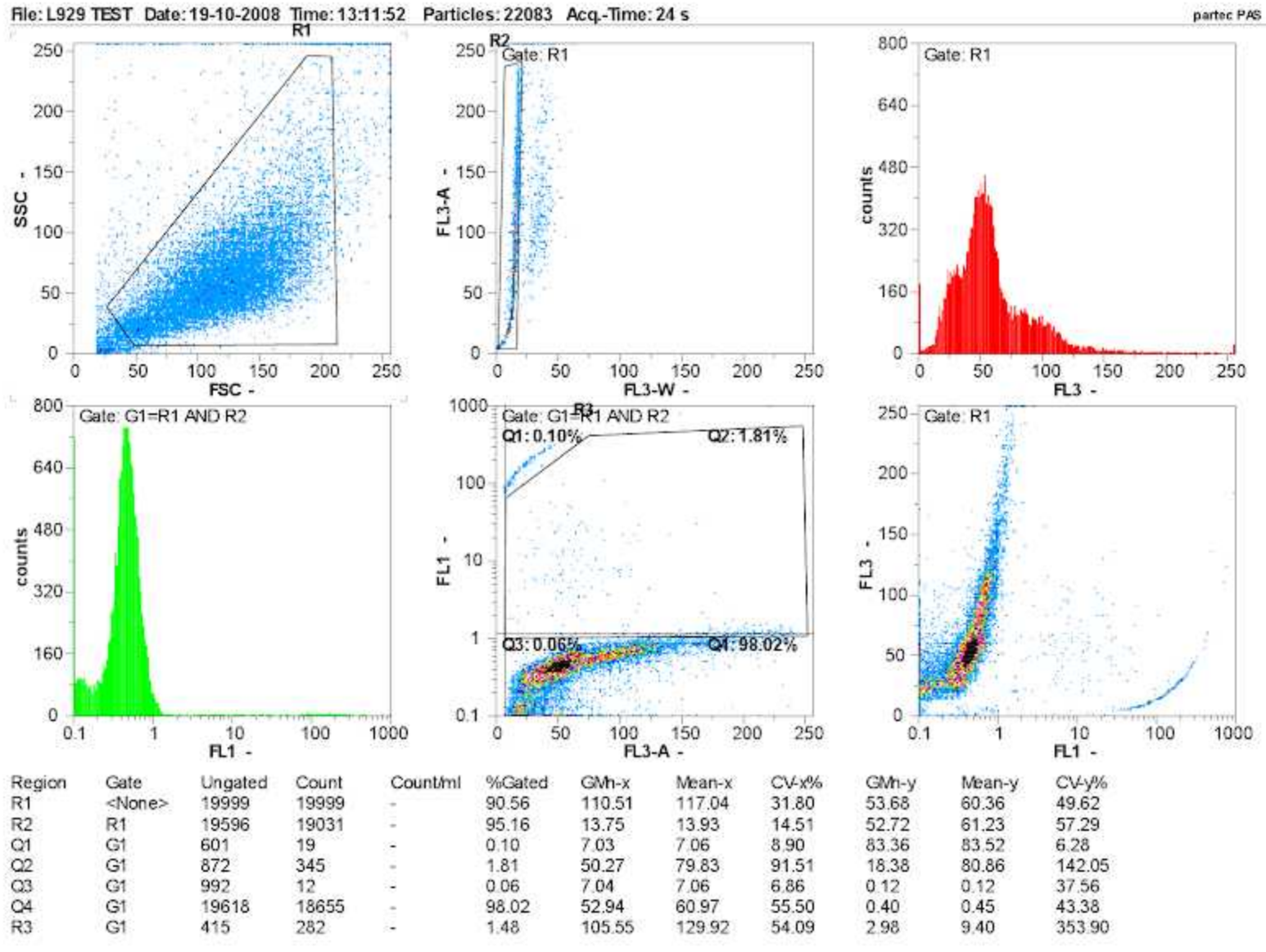

Region	Gate	Ungated	Count	Count/ml	%Gated	GMn-x	Mean-x	CV-x%	GMn-y	Mean-y	CV-y%
R1	<None>	19999	19999	-	90.56	110.51	117.04	31.80	53.68	60.36	49.62
R2	R1	19596	19031	-	95.16	13.75	13.93	14.51	52.72	61.23	57.29
Q1	G1	601	19	-	0.10	7.03	7.06	8.90	83.36	83.52	6.28
Q2	G1	872	345	-	1.81	50.27	79.83	91.51	18.38	80.86	142.05
Q3	G1	992	12	-	0.06	7.04	7.06	6.86	0.12	0.12	37.56
Q4	G1	19618	18655	-	98.02	52.94	60.97	55.50	0.40	0.45	43.38
R3	G1	415	282	-	1.48	105.55	129.92	54.09	2.98	9.40	353.90

(b)

Figure 1: Flow cytometry results for L929 Cells (a) with no SPION added and (b) with SPION (iron concentration of 200 mM) added; with permission from reference [12].

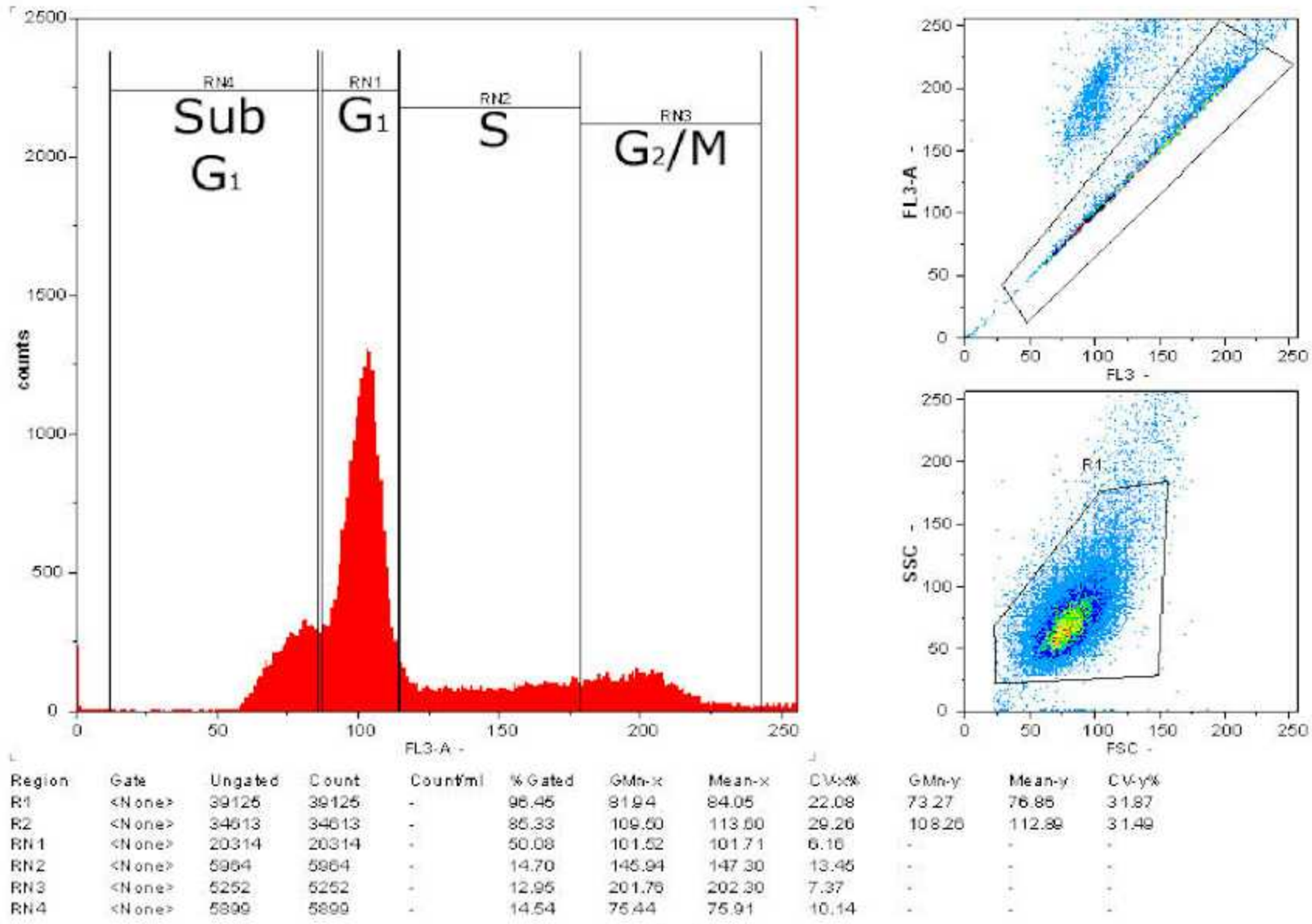

Region	Gate	Ungated	Count	Count/ml	%Gated	GMn-x	Mean-x	CV-x%	GMn-y	Mean-y	CV-y%
R1	<None>	39125	39125	-	96.45	81.94	84.05	22.08	73.27	76.85	31.87
R2	<None>	34613	34613	-	85.33	109.60	113.00	29.26	108.26	112.89	31.49
RN1	<None>	20314	20314	-	50.08	101.52	101.71	6.16	-	-	-
RN2	<None>	5964	5964	-	14.70	145.94	147.30	13.45	-	-	-
RN3	<None>	5252	5252	-	12.95	201.76	202.30	7.37	-	-	-
RN4	<None>	5899	5899	-	14.54	75.44	75.91	10.14	-	-	-

(a)

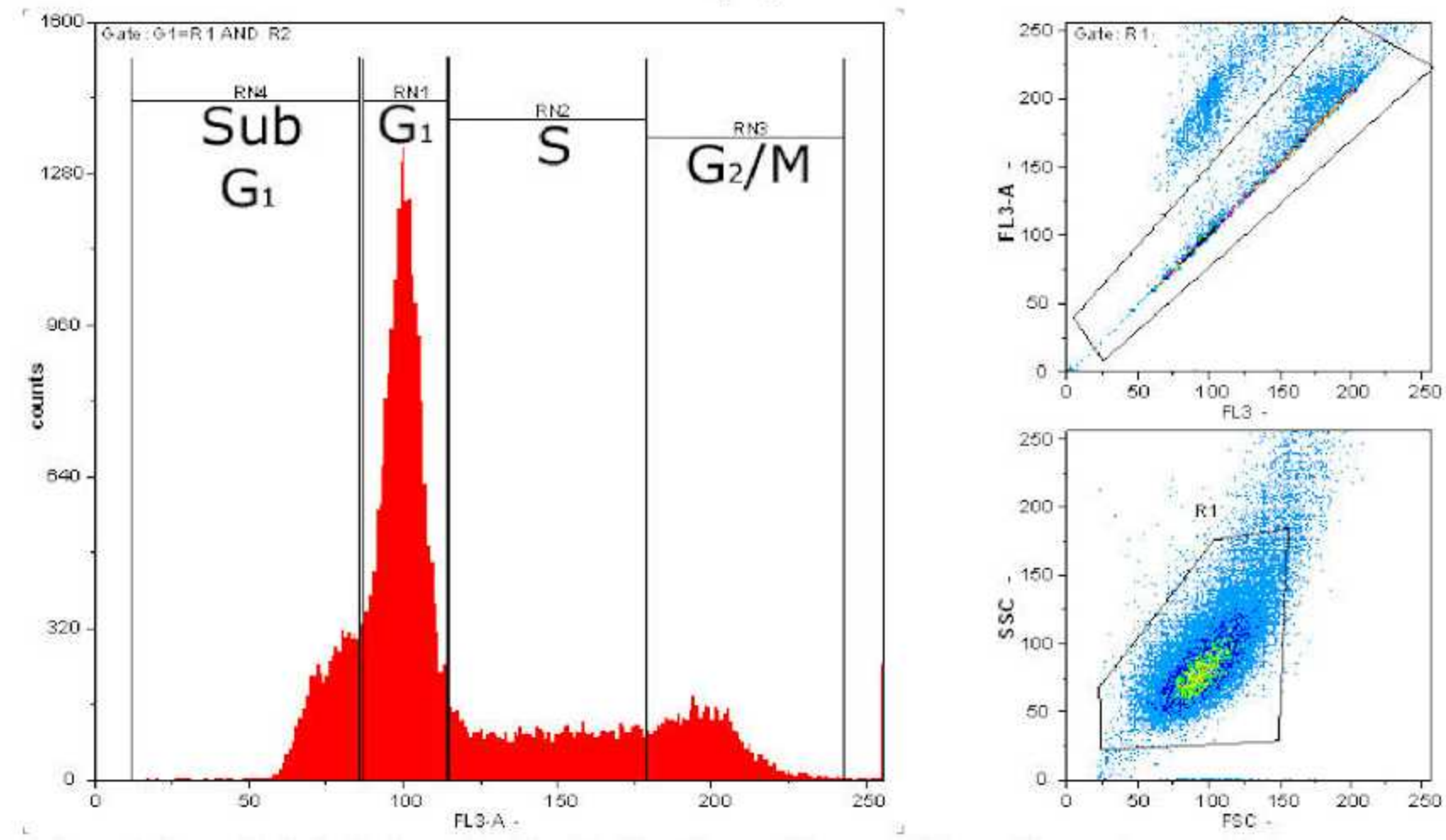

Region	Gate	Ungated	Count	Count/ml	%Gated	GMn-x	Mean-x	CV-x%	GMn-y	Mean-y	CV-y%
R1	<None>	42199	42199	-	94.26	98.06	100.45	21.34	85.51	89.32	29.99
R2	R1	37890	37286	-	88.36	112.40	117.27	30.90	112.90	118.80	34.36
RN1	G1	20131	20090	-	53.88	100.30	100.50	6.22	-	-	-
RN2	G1	7223	6675	-	17.90	145.46	146.76	13.18	-	-	-
RN3	G1	7266	4836	-	12.97	198.53	198.91	6.25	-	-	-
RN4	G1	5574	5560	-	14.91	76.02	76.42	9.60	-	-	-

(b)

Figure 2: Cell cycle assay results for (a) control and (b) coated SPION (200 mM) treated cells; with permission from reference [13].

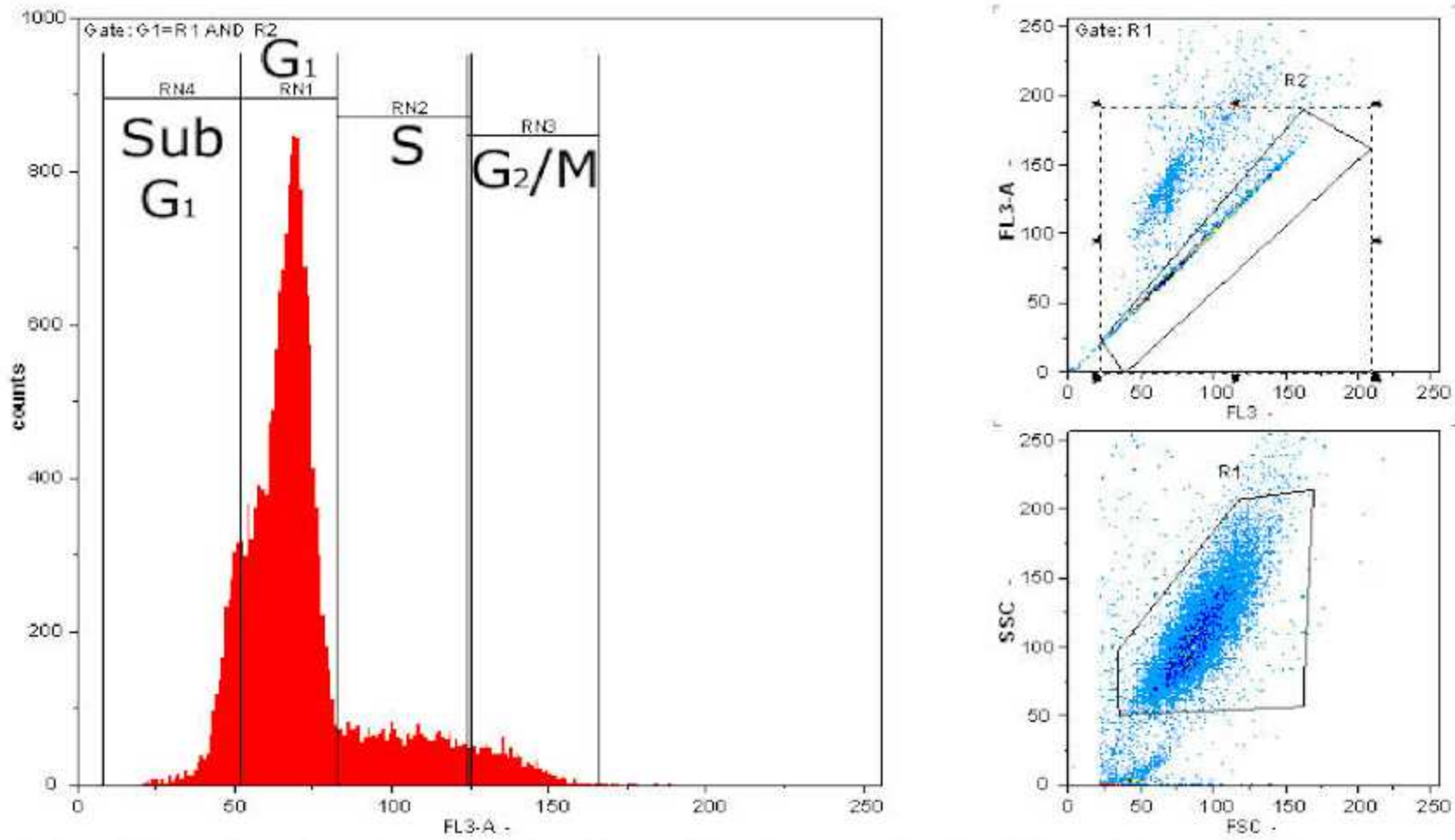

Region	Gate	Ungated	Count	Count/ml	%Gated	GMn-x	Mean-x	CV-x%	GMn-y	Mean-y	CV-y%
R1	<None>	22526	22526	-	84.51	90.60	92.60	20.44	108.04	111.80	26.17
R2	R1	20957	20529	-	91.13	71.90	74.43	28.32	70.24	73.09	30.58
RN1	G1	14758	14479	-	70.53	66.70	67.08	10.54	-	-	-
RN2	G1	3194	2718	-	13.24	102.49	103.20	11.67	-	-	-
RN3	G1	2078	1041	-	5.07	137.07	137.33	6.26	-	-	-
RN4	G1	2510	2364	-	11.52	46.54	46.90	11.21	-	-	-

(a)

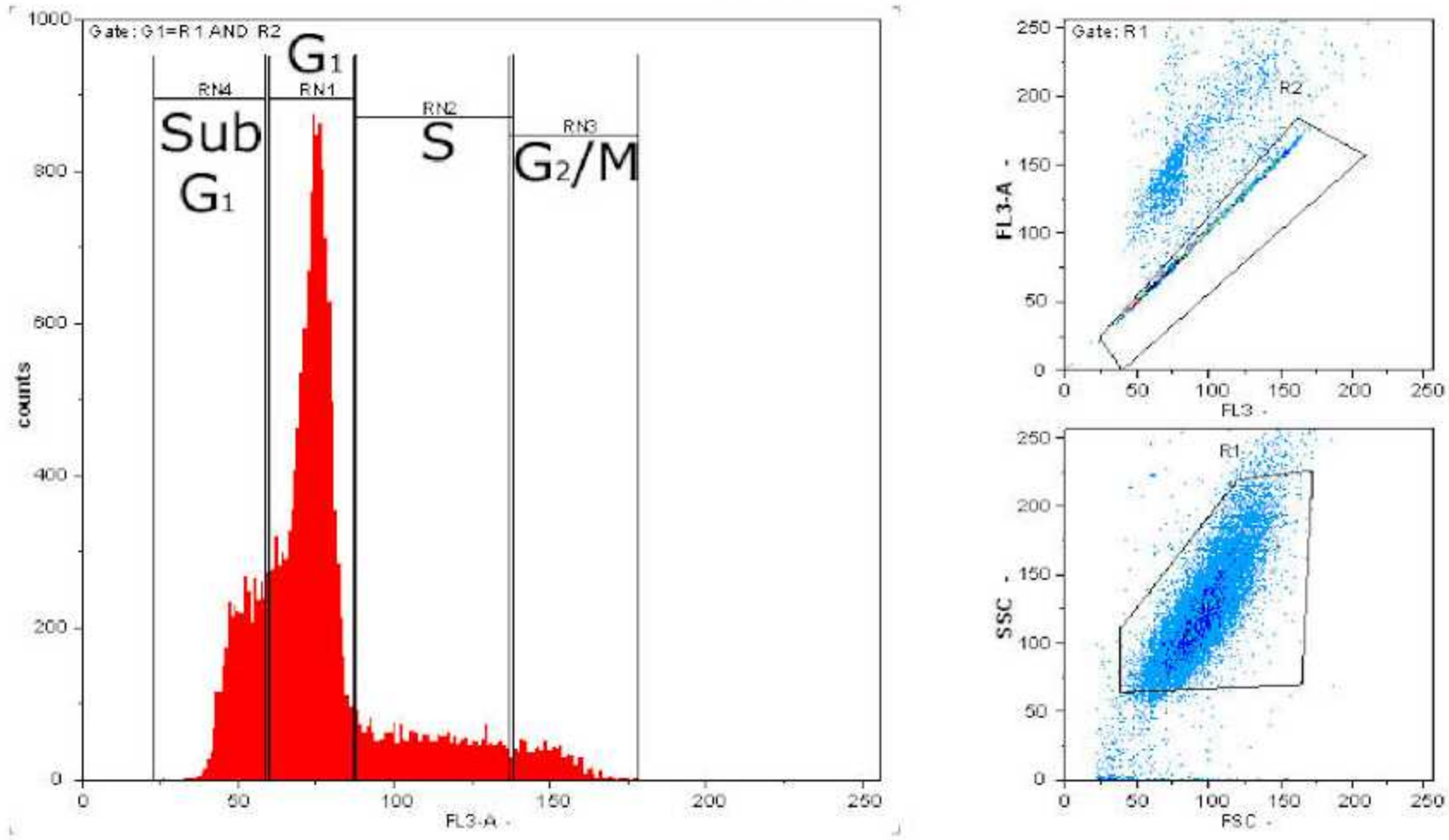

Region	Gate	Ungated	Count	Count/ml	%Gated	GMn-x	Mean-x	CV-x%	GMn-y	Mean-y	CV-y%
R1	<None>	22673	22673	-	93.96	95.96	98.13	20.61	120.58	124.85	26.42
R2	R1	20722	19978	-	88.11	76.08	78.96	29.33	75.17	78.42	31.46
RN1	G1	12394	12210	-	61.12	73.73	73.98	8.17	-	-	-
RN2	G1	3748	2842	-	14.23	110.21	111.16	13.05	-	-	-
RN3	G1	2268	960	-	4.81	150.04	150.26	5.43	-	-	-
RN4	G1	4110	3738	-	18.71	51.42	51.67	9.76	-	-	-

(b)

Figure 3: Cell cycle assay results for (a) control and (b) coated SPION (400 mM) treated cells; with permission from reference [13].

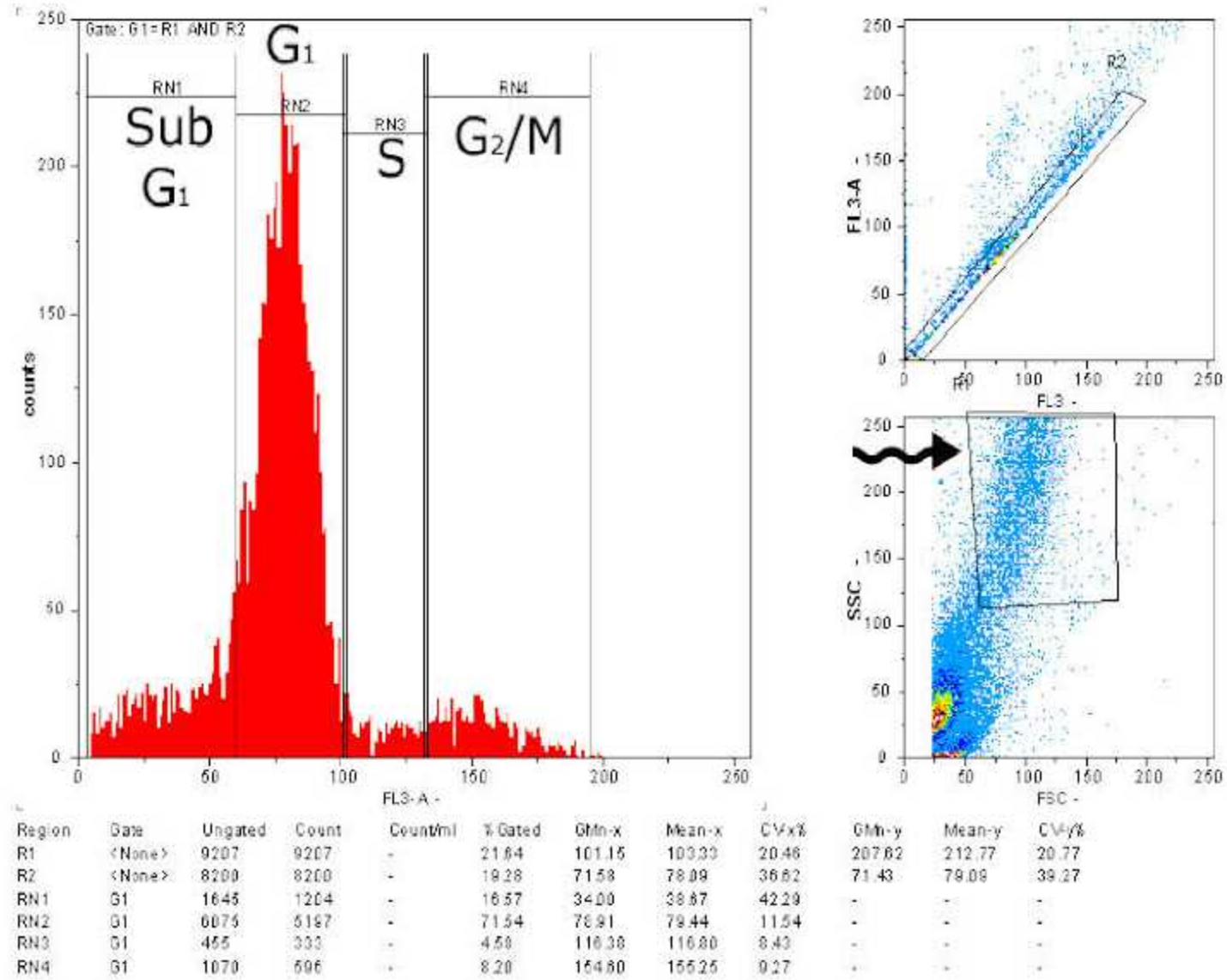

Region	Gate	Ungated	Count	Count/ml	%Gated	GMn-x	Mean-x	CV-x%	GMn-y	Mean-y	CV-y%
R1	<None>	9207	9207	-	21.64	101.15	103.33	20.46	207.62	212.77	20.77
R2	<None>	8200	8200	-	19.28	71.58	78.09	36.62	71.43	79.09	39.27
RN1	G1	1645	1204	-	16.57	34.00	38.87	42.29	-	-	-
RN2	G1	6075	5187	-	71.54	78.91	79.44	11.54	-	-	-
RN3	G1	455	333	-	4.58	116.38	116.80	8.43	-	-	-
RN4	G1	1070	596	-	8.20	154.60	155.25	9.27	-	-	-

(a)

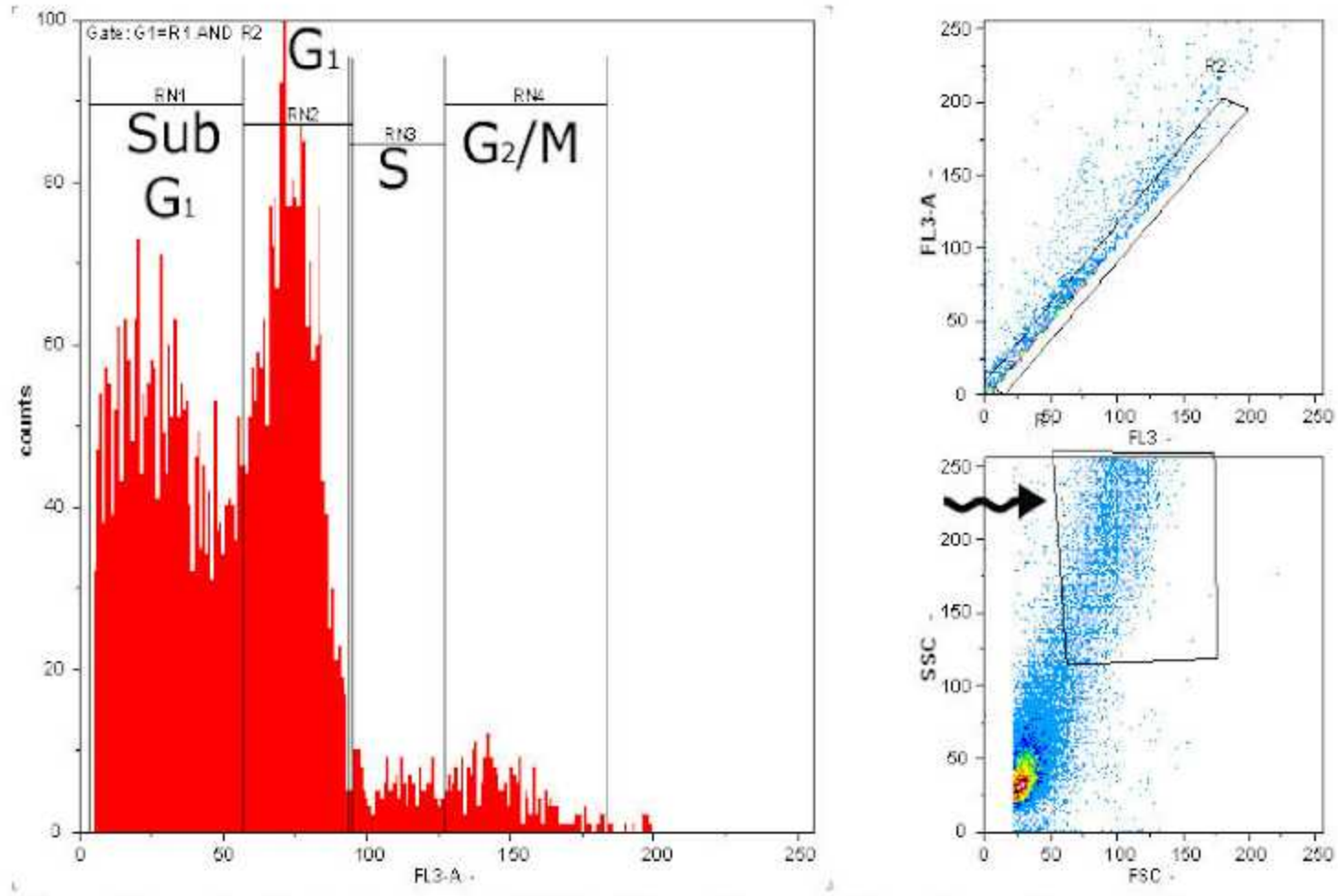

Region	Gate	Ungated	Count	Count/ml	%Gated	GMn-x	Mean-x	CV-x%	GMn-y	Mean-y	CV-y%
R1	<None>	7430	7430	-	23.40	101.00	103.29	20.73	216.22	220.93	19.08
R2	<None>	5603	5603	-	17.65	47.16	56.51	55.41	45.49	56.80	59.99
RN1	G1	3087	2553	-	49.96	25.87	30.08	48.93	-	-	-
RN2	G1	2576	2148	-	42.04	73.08	73.61	12.06	-	-	-
RN3	G1	323	184	-	3.60	109.86	110.27	8.56	-	-	-
RN4	G1	571	251	-	4.91	146.41	146.98	8.94	-	-	-

(b) Increasing Granulity

Figure 4: Cell cycle assay results for treated cells to uncoated SPION with concentration of (a) 200 and (b) 400 mM; with permission from reference [13].

In order to track the effects of both bare and PVA coated SPION on the L929 cells, this method has been applied. Cell cycle assessment was carried out by staining of the DNA with PI followed by flow cytometric measurement [13]. Approximately 10^6 L929 cells were cultured and treated with SPION with concentrations of 100, 200 and 400 mM of iron for 72 h. The effects of SPION treated cells were probed in each phase of the cell cycle and compared with control cells. According to the obtained results, both bare and PVA coated SPION with the iron concentration of 100 and 200 mM have no detectable effect on the cell life cycle phases and were similar to the control cells (see Figs. **2** and **4**).

The same proportion of the cell population in $subG_1$ phase in control cells and SPION treated cells confirmed the absence of apoptosis. As the concentration of coated-SPION increased with an iron concentration of 400 mM, a negligible amount of apoptosis was observed in the assay (see Fig. **3**). In contrast, for the bare SPION treated cells, a significant increase in the proportion of apoptotic cells ($\Delta SubG_1/SubG_1(control)$ =0.62) was observed (see Fig. **4**) due to the irreversible DNA damage. In addition to apoptosis, the arrest in the G_0G_1 phase was detected for the bare SPION treated cells at an iron concentration of 400 mM. Furthermore, due to the higher surface activity of the bare SPION in comparison with the PVA coated particles, the granularity of the bare SPION treated-cells was increased, which is clearly shown in Fig. **4b**.

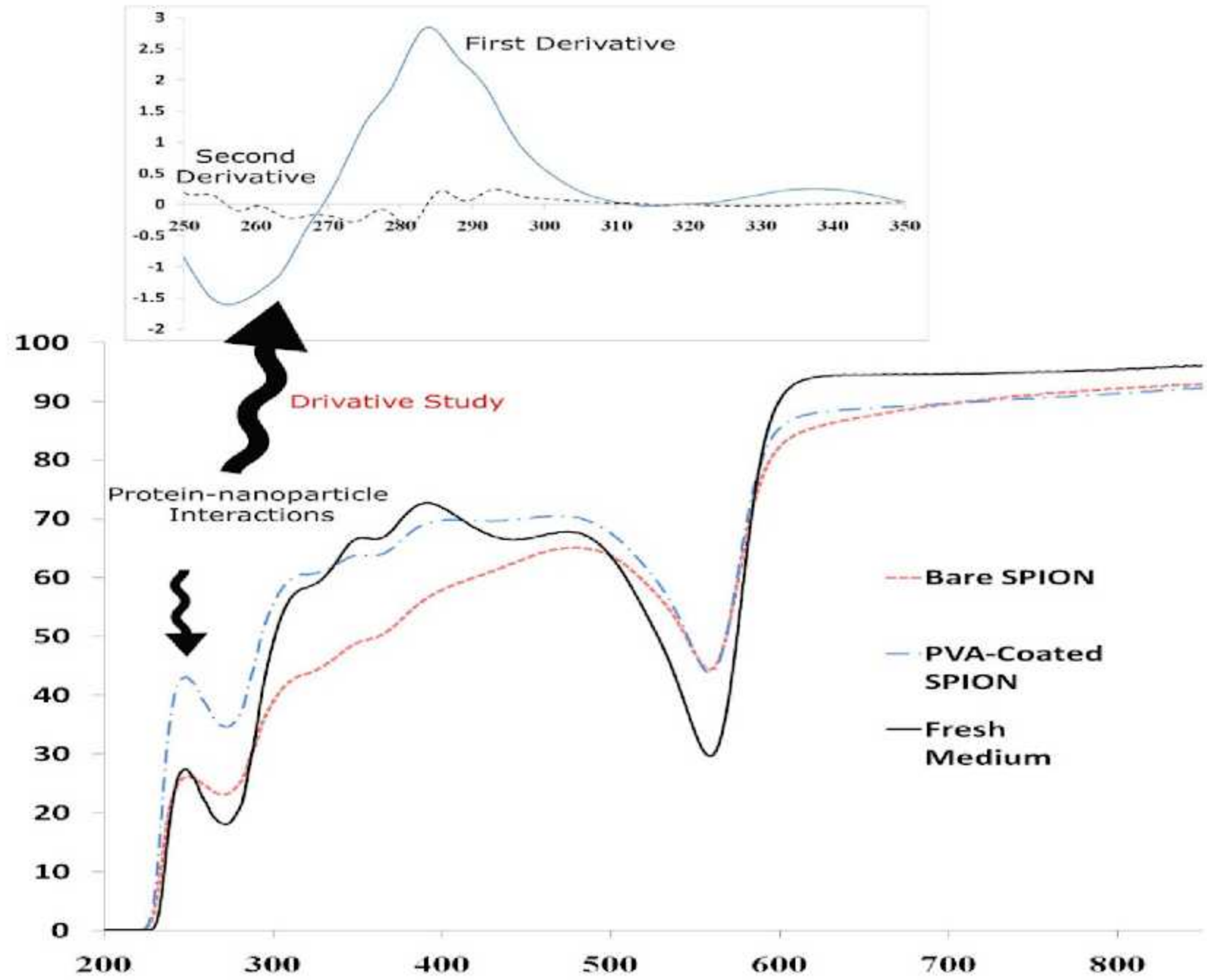

Figure 5: UV/Vis spectra of fresh cell medium, the extract medium of uncoated and coated SPION (DI water defined as reference in UV/Vis spectrum). Upper graph: first (solid line) and second (dash-line) order derivatives of coated SPION (with iron concentration of 400 mM); with permission from reference [13].

PROTEIN-SPION INTERACTIONS AND THEIR EFFECTS ON CELL CYCLE ASSAY

It is now well-recognized that the NPs can interact with proteins on their entrance into the biological environment [30-34]. The outcome of these interactions may cause the malfunction of the crucial proteins

that could have a significant effect on the cell life cycle. *In vitro* investigations have shown that SPION can interaction with cell medium containing fetal bovine serum (FBS) whereby the particles demonstrate adsorption of FBS proteins to the surface of the SPION. More specifically, the UV/Vis spectroscopy of both fresh cell medium and extracted medium after interactions with bare and coated (PVA and PEGF) SPION confirmed not only protein absorption but also pH changes (at wavelength of 560 nm in the spectra) of the cell culture which can cause severe errors in toxicity evaluation methods (*e.g.*, MTT (3-(4,5-dimethylthiazol-2-yl)-2,5-diphenyltetrazolium bromide) assay) [13, 15, 16]. Fig. **5** shows the effect of uncoated and PVA-coated SPION on the cell medium. In addition to PVA, the effect of PEGF coated SPION on the cell medium were probed and similar results were obtained (Fig. **6**).

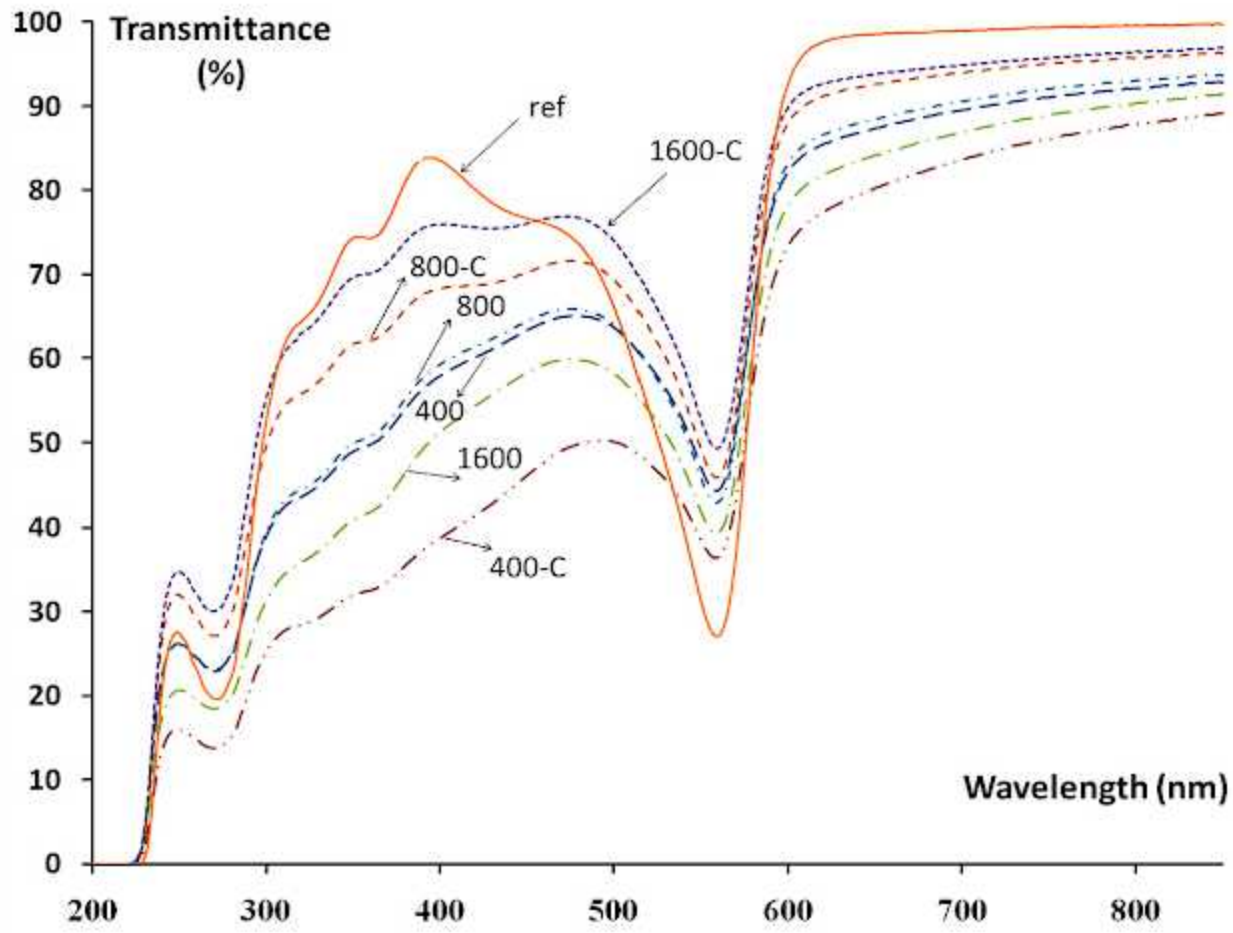

Figure 6: UV/Vis spectra of 'pure' cell medium (ref), the extract of coated (C) and bare SPION with de-ionized (DI) water as the reference in UV/Vis spectrum. (The numbers are concentrations of iron in mM, C refers to coated nanoparticles); with permission from reference [15].

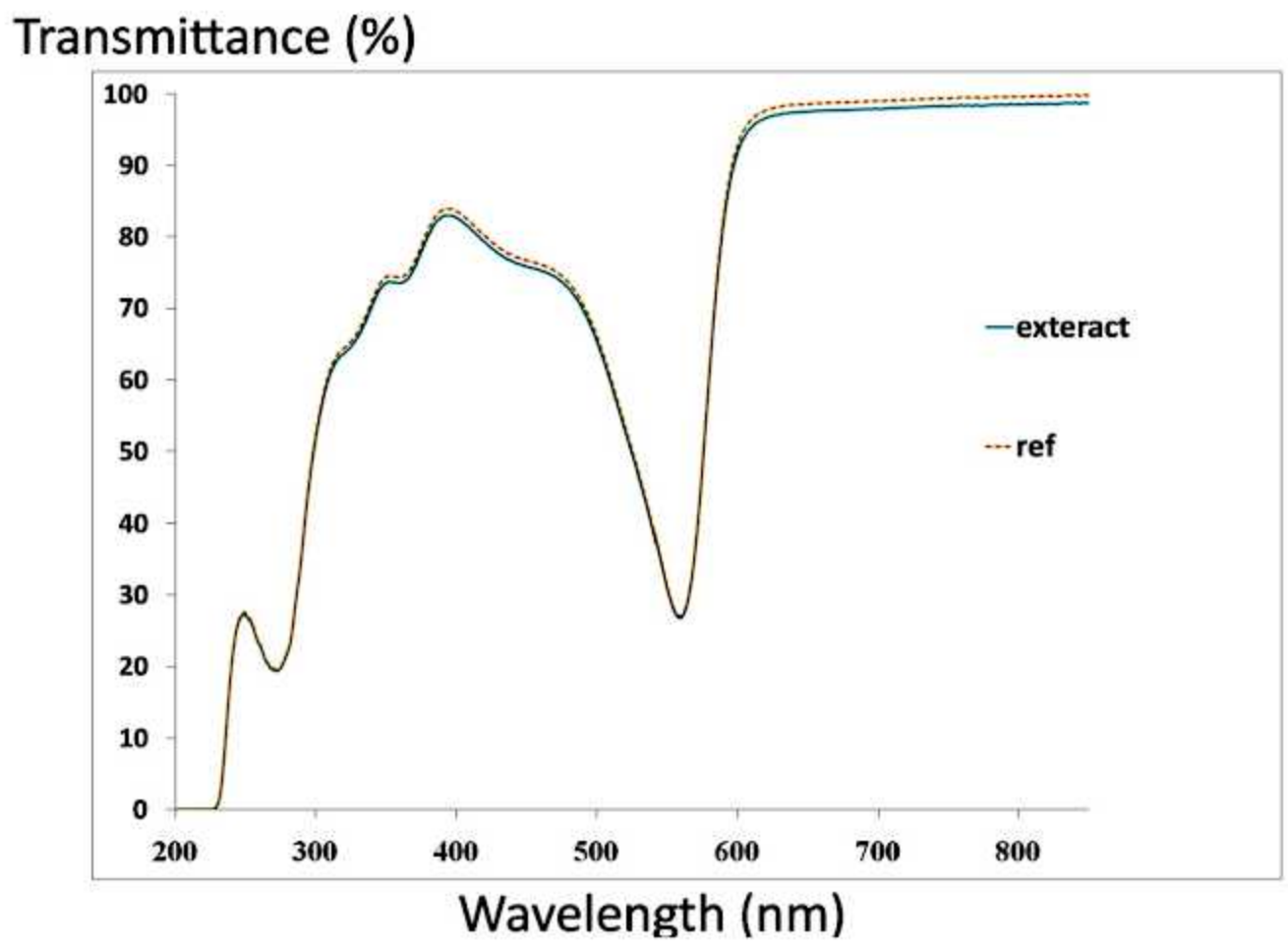

Figure 7: UV/Vis spectra of pure cell medium (ref) and the extract of surface saturated SPION; with permission from reference [15].

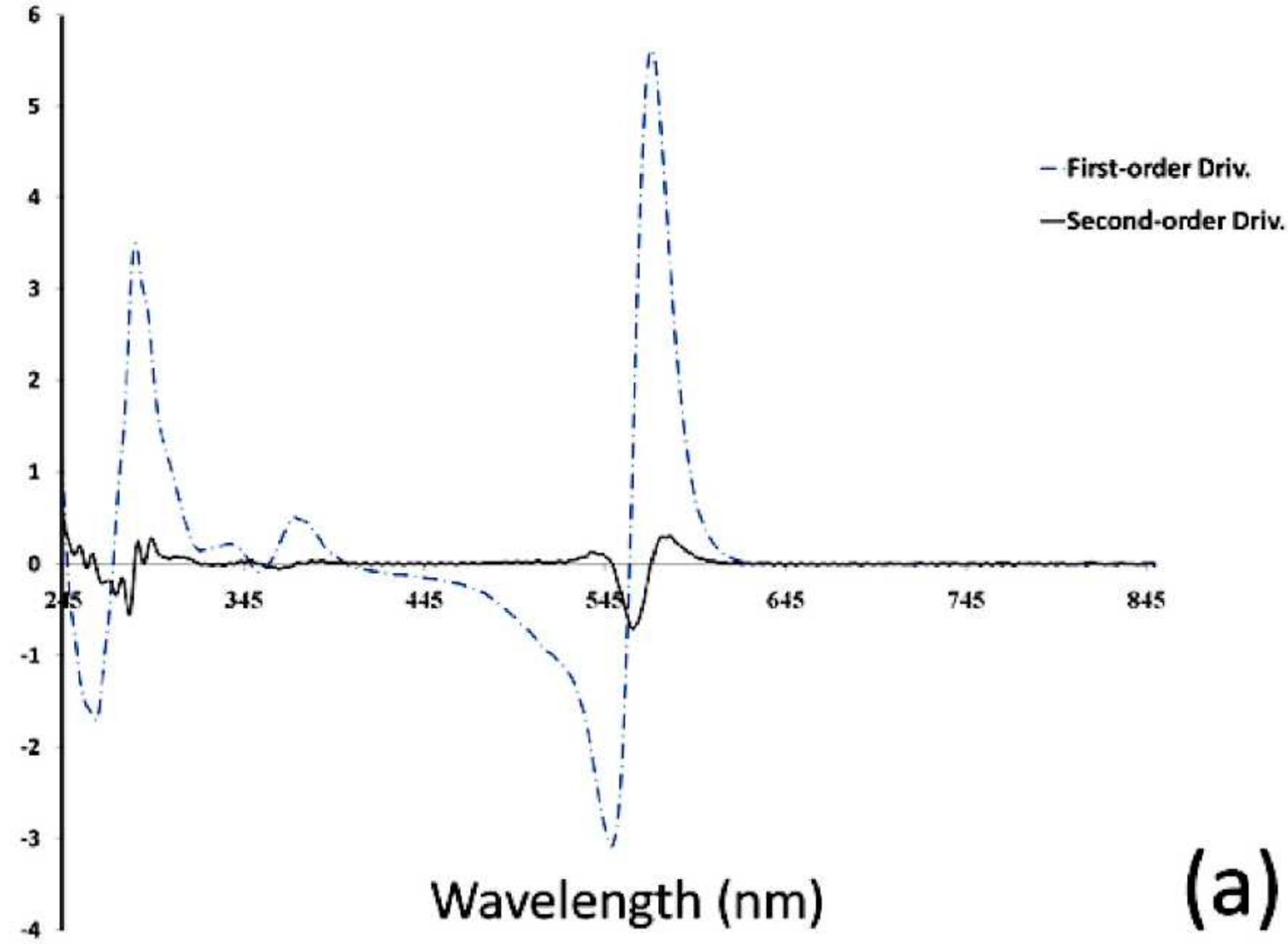

(a)

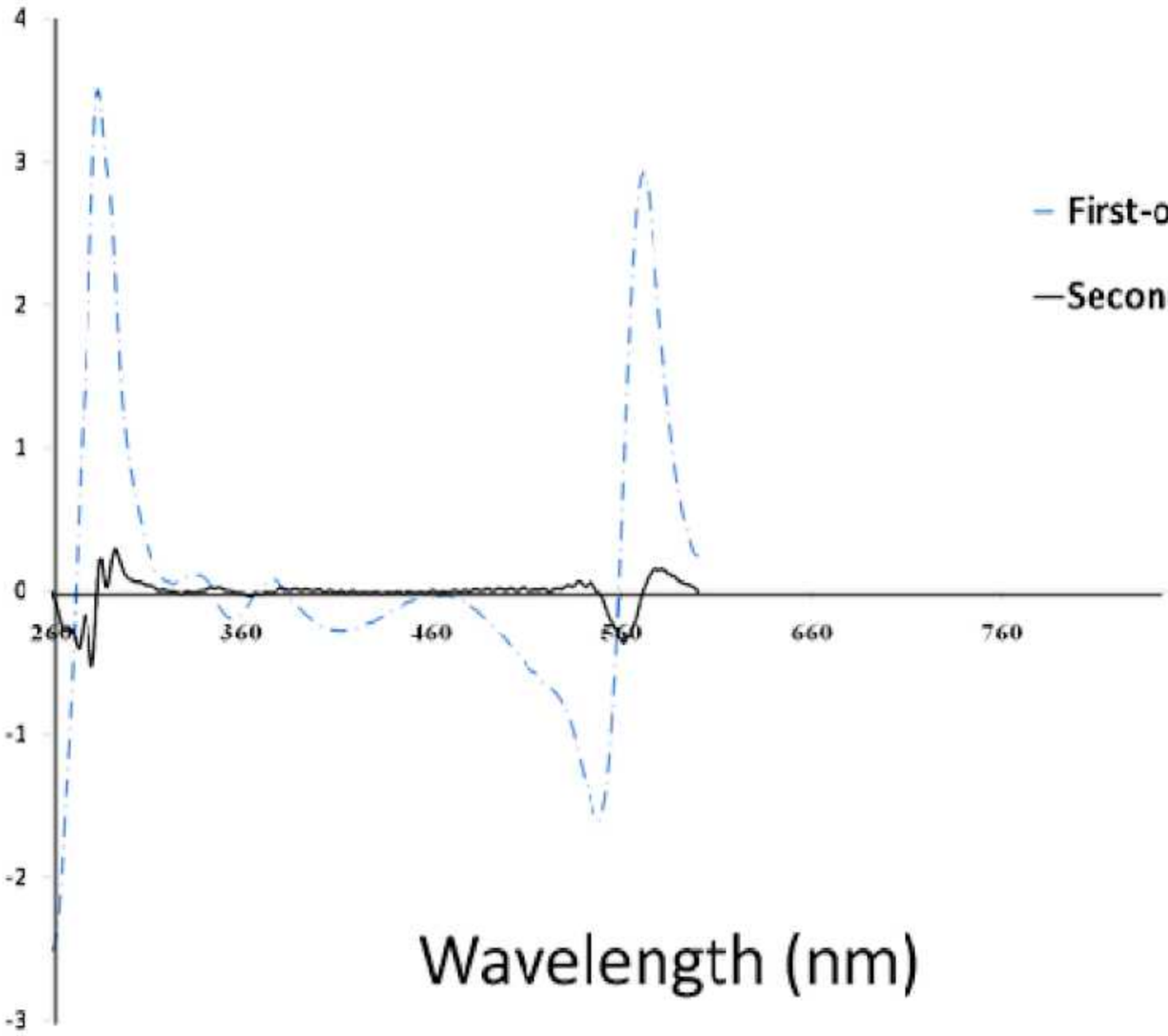

(b)

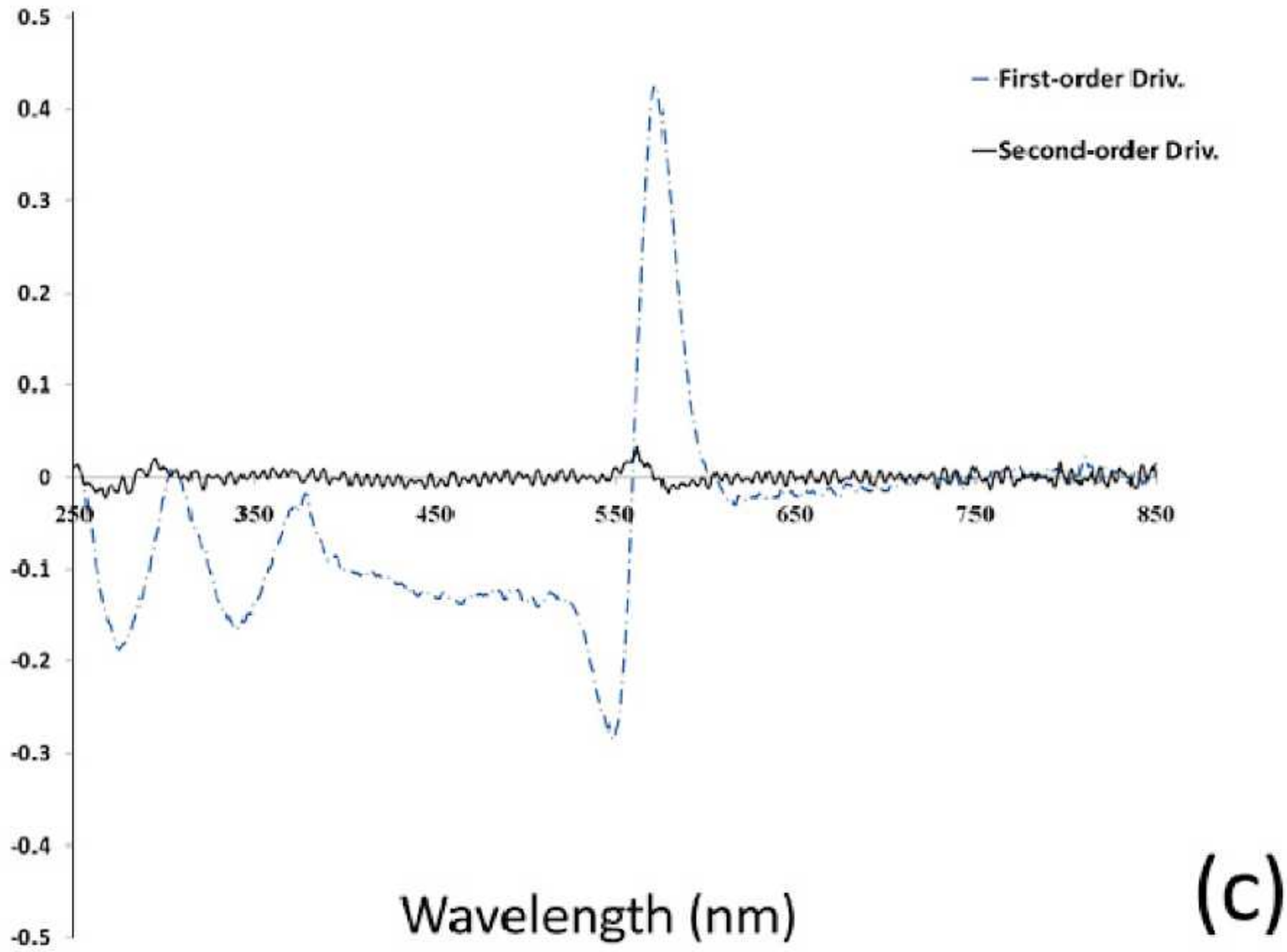

Figure 8: First (dash-line) and second (solid line) order derivatives of (a) 1600B, (b) 1600C, and (c) 1600CM (modified sample); with permission from reference [15].

To overcome this problem, a modified method has been proposed using the following steps: (1) introduction of the nanoparticles to the cell medium, (2) incubation of the solution for 24 hours in order to create a hard protein corona, (3) replacing the medium with a fresh one, and (4) application of the surface saturated SPION to the assays [13, 15, 16]. By applying this protocol, the obtained SPION did not change the spectra of the cell medium (see Fig. **7**), resulting a more appropriate toxicity evaluations of the NPs.

In order to prove that the adsorption of several proteins to the surface of SPION occurs, the derivative spectroscopy method was employed [13, 15, 16]. Both first and second order derivatives have been probed for detection of multi-component changes in cell culture medium following interaction with SPION. The results are shown in Fig. **8**. Multi-protein absorbance is detected *via* the second derivative curves between the wavelengths of 250-300 nm in both bare and PEGF-coated SPION (Figs. **8a** and **b**). Fig. **8c** shows the derivative curves for the modified samples, denoting negligible absorbance at aforementioned wavelengths. By applying this new protocol to the L929 cell lines, the observed irreversible DNA damages are decreased leading to the reduction of apoptosis of the cells at the same concentrations [7].

LIST OF ABBREVIATIONS

NPs: Nanoparticles; SPION: Superparamagnetic Iron Oxide Nanoparticles; MRI: Magnetic Resonance Imaging; ROS: Reactive Oxygen Species; TUNEL: Terminal deoxynucleotidyl transferase-mediated dUTP nick end-labeling; PVA: PolyVinyl Alcohol; PI: Propidium Iodide; PBS: Phosphate Buffer Saline; FBS: Fetal Bovine Serum; PEGF: PolyEthylene Glycol Fumarate; MTT: 3-(4,5-dimethylthiazol-2-yl)-2,5-diphenyltetrazolium bromide

REFERENCES

[1] Smith JA, Martin L. Do cells cycle? Proc Natl Acad Sci USA 1973; 70 (4): 1263-1270.

[2] Morgan DO. The Cell Cycle: Principles of Control. London, New Science Press in association with Oxford University Press 2007.

[3] Lewin B, Cassimeris L, Lingappa VR. Cells, Jones & Bartlett Publishers 2007.

[4] Alberts B, Johnson A, Lewis J, Raff M, Roberts K, Walter P. Molecular Biology of the Cell (5th ed.). New York: Garland Science 2008.

[5] Alberts B, Bray D, Johnson A, *et al.* Essential Cell Biology: An Introduction to the Molecular Biology of the Cell Garland Publishing, New York 1997.

[6] Nel AE, Madler L, Velegol D, *et al.* Understanding biophysicochemical interactions at the nano-bio interface. Nat Mater 2009; 8: 543-557.

[7] Mahmoudi M, Simchi A, Vali H, *et al.* Cytotoxicity and cell cycle effects of bare and polyvinyl alcohol coated iron oxide nanoparticles in mouse fibroblasts Adv Eng Mater 2009; 11 (12): B243-B250.

[8] Ishikawa K, Ishii H, Saito T. DNA Damage-Dependent Cell Cycle Checkpoints and Genomic Stability. DNA Cell Biol 2006; 25: 406-411.

[9] Gupta AK, Gupta M, Cytotoxicity suppression and cellular uptake enhancement of surface modified magnetic nanoparticles. Biomaterials 2005; 26: 1565-1573.

[10] Gupta AK, Naregalkar RR, Vaidya VD, Gupta M. Recent advances on surface engineering of magnetic iron oxide nanoparticles and their biomedical applications. Nanomedicine 2007; 2 (1): 23-39.

[11] Mahmoudi M, Simchi A, Imani M. Recent advances in surface engineering of superparamagnetic iron oxide nanoparticles for biomedical applications. J Iranian Chem Soc 2010; 7 (3): 1-27.

[12] Mahmoudi M, Shokrgozar MA, Simchi A, *et al.* Multiphysics Flow Modeling and *in vitro* Toxicity of Iron Oxide Nanoparticles Coated with Poly(vinyl alcohol). J Phys Chem C 2009; 113 (6): 2322-2331.

[13] Mahmoudi M, Simchi A, Imani M. Cytotoxicity of Uncoated and Polyvinyl Alcohol Coated Superparamagnetic Iron Oxide Nanoparticles. J Phys Chem C 2009; 113 (22): 9573-9580.

[14] Mahmoudi M, Simchi A, Imani M, Hafeli UO. Superparamagnetic Iron Oxide Nanoparticles with Rigid Cross-linked Polyethylene Glycol Fumarate Coating for Application in Imaging and Drug Delivery. J Phys Chem C 2009; 113 (19): 8124-8131.

[15] Mahmoudi M, Simchi A, Imani M, Milani AS, Stroeve P. An *in vitro* study of bare and poly(ethylene glycol)-co-fumarate-coated superparamagnetic iron oxide nanoparticles: a new toxicity identification procedure. Nanotechnology 2009; 20 (22): 225104.

[16] Mahmoudi M, Simchi A, Imani M, *et al.* A new approach for the *in vitro* identification of the cytotoxicity of superparamagnetic iron oxide nanoparticles. Colloid Surf B 2010; 75: 300-309.

[17] Mahmoudi M, Simchi A, Milani AS, Stroeve P. Cell toxicity of superparamagnetic iron oxide nanoparticles. J Colloid Interface Sci 2009; 336: 510-518.

[18] Mahmoudi M, Hosseinkhani H, Hosseinkhani M, *et al.* MRI tracking of stem cells *in vivo* using iron oxide nanoparticles as a tool for the advancement of clinical regenerative medicine. Chem Rev 2011; 111 (2): 253-280.

[19] Mahmoudi M, Milani AS, Stroeve P. Surface Architecture of Superparamagnetic Iron Oxide Nanoparticles for Application in Drug Delivery and Their Biological Response: A Review. Int J Biomedical Nanoscience and Nanotechnology 2010; 1(2/3/4/): 164-201.

[20] Mahmoudi M, Sant S, Wang B, *et al.* Superparamagnetic Iron Oxide Nanoparticles (SPION): Development, surface modification and applications in chemotherapy. Adv Drug Delivery Rev 2011; 63(1-2): 24-46.

[21] Cunningham CH, Arai T, Yang PC, *et al.* Positive contrast magnetic resonance imaging of cells labeled with magnetic nanoparticles. Magn Res Med 2005; 53 (5): 999-1005.

[22] Anderson SA, Rader RK, Westlin WF, *et al.* Magnetic resonance contrast enhancement of neovasculature with alpha(v)beta(3)-targeted nanoparticles. Magn Res Med 2000; 44 (3): 433-439.

[23] Polyak B, Friedman G. Magnetic targeting for site-specific drug delivery: applications and clinical potential. Exp Opin Drug Delivery 2009; 6 (1): 53-70.

[24] Jalilian AR, Panahifar A, Mahmoudi M, Akhlaghi M, Simchi A. Preparation and biological evaluation of [67Ga]-labeled- superparamagnetic nanoparticles in normal rats. Radiochim Acta 2009; 97 (1): 51-56.

[25] Bartolozzi C, Lencioni R, Donati F, Cioni D. Abdominal MR: Liver and pancreas. Europ Radiol 1999; 9 (8): 1496-1512.

[26] Meng J, Fan J, Galiana G, *et al.* LHRH-functionalized superparamagnetic iron oxide nanoparticles for breast cancer targeting and contrast enhancement in MRI. Mater Sci Eng C 2009; 29 (4): 1467-1479.

[27] Karlsson HL, Cronholm P, Gustafsson J, Moller L. Copper oxide nanoparticles are highly toxic: A comparison between metal oxide nanoparticles and carbon nanotubes. Chem Res Toxicol 2008; 21: 1726-1732.

[28] Saleh OA, Blalock WL, Burrows C, *et al.* Enhanced ability of the progenipoietin-1 to suppress apoptosis in human hematopoietic cells. Int J Mol Med 2002; 10 (4): 385-394.

[29] Reinhold WC, Kouros-Mehr H, Kohn KW, *et al.* Apoptotic susceptibility of cancer cells selected for camptothecin resistance: Gene expression profiling, functional analysis, and molecular interaction mapping. Cancer Res 2003; 63 (5): 1000-1011.

[30] Cedervall T, Lynch I, Foy M, *et al.* Detailed Identification of Plasma Proteins Adsorbed on Copolymer Nanoparticles. Ang Chem Int Ed 2007; 46: 5754 -5756.

[31] Cedervall T, Lynch I, Lindman S, *et al.* Understanding the nanoparticle-protein corona using methods to quantify exchange rates and affinities of proteins for nanoparticles. Proc Nat Acad Sci USA 2007; 104 (7): 2050-2055.

[32] Lundqvist M, Stigler J, Elia G, Lynch I, Cedervall T, Dawson KA. Nanoparticle size and surface properties determine the protein corona with possible implications for biological impacts. Proc Nat Acad Sci USA 2008; 105 (38): 14265-14270.

[33] Lynch I, Cedervall T, Lundqvist M, Cabaleiro-Lago C, Linse S, Dawson KA, The nanoparticle-protein complex as a biological entity; a complex fluids and surface science challenge for the 21st century. Adv Colloid Interface Sci 2007; 134-135: 167-174.

[34] Lynch I, Dawson KA, Linse S. Detecting Cryptic Epitopes Created by Nanoparticles. Science 2006; 327: 14.

[35] Huang DM, Hsiao JK, Chen YC, *et al.* The promotion of human mesenchymal stem cell proliferation by superparamagnetic iron oxide nanoparticles. Biomaterials 2009; 30 (22): 3645-3651.